Quantum phase diagram of a frustrated spin-$\frac{1}{2}$ system on a trellis ladder

Debasmita Maiti* and Manoranjan Kumar†

S. N. Bose National Centre for Basic Sciences, Block JD, Sector III, Salt Lake, Kolkata 700106, India

(Received 12 September 2019; revised manuscript received 21 November 2019; published 10 December 2019)

We study an isotropic Heisenberg spin-$\frac{1}{2}$ model on a trellis ladder which is composed of two $J_1 - J_2$ zigzag ladders interacting through antiferromagnetic rung coupling J_3. J_1 and J_2 are ferromagnetic zigzag spin interaction between two legs and antiferromagnetic interaction along each leg of a zigzag ladder. A quantum phase diagram of this model is constructed using the density matrix renormalization group method and linearized spin-wave analysis. In the small J_2 limit, a short-range striped collinear phase is found in the presence of J_3, whereas, in the large J_2/J_3 limit, a noncollinear quasi-long-range phase is found. The system shows a short-range noncollinear state in the large J_3 limit. The short-range-order phase is the dominant feature of this phase diagram. We also show that the results obtained by DMRG and linearized spin-wave analysis show a similar phase boundary between the collinear striped and noncollinear short-range phases, and the collinear phase region shrinks with increasing J_3. We apply this model to understand the magnetic properties of CaV_2O_5 and also fit the experimental data of susceptibility and magnetization. We note that J_3 is a dominant interaction in this material, whereas J_1 and J_2 are approximately half of J_3. The variation of magnetic specific heat capacity as a function of temperature for various external magnetic fields is also predicted.

DOI: 10.1103/PhysRevB.100.245118

I. INTRODUCTION

In the last couple of decades, frustrated low-dimensional quantum magnets have been intensively explored in search of various exotic phases like spin fluid with quasi-long-range order (QLRO) [1–6], spin dimer with short-range order (SRO) [2,3,7–9], vector chiral [10,11], multipolar phases [10–13], etc. These phases arise in the presence of some specific types of spin-exchange interactions which may enhance the quantum fluctuations in low-dimensional frustrated systems like one-dimensional (1D) spin chains realized in materials, $LiCuVO_4$ [14], Li_2CuZrO_4 [15], Li_2CuSbO_4 [16], $(N_2H_5)CuCl_3$ [17], etc., and quasi-1D spin ladders manifested in the form of $SrCu_2O_3$ [18], $(VO)_2P_2O_7$ [19,20], etc. Frustrated twisted ladders are also realized in materials like $Ba_3Cu_3In_4O_{12}$ and $Ba_3Cu_3Sc_4O_{12}$ [21–24]. A majority of the 1D frustrated magnetic systems mentioned above are modeled by a simple J_1-J_2 chain [1,3–8,15,25–33]. This model can explain the gapless spin fluid [1,4], gapped dimer [3,7], gapped noncollinear (NC) [3–6], and decoupled phases [34].

In fact, many of these 1D systems like $LiCuVO_4$ [14] and Li_2CuZrO_4 [15] show three-dimensional ordering at low temperature; therefore, interchain couplings are considered to understand the interesting physics below the three-dimensional ordering temperature. However, there are materials with effective spin interactions confined to a quasi-1D ladderlike structure, e.g., $SrCu_2O_3$ [18], $(VO)_2P_2O_7$ [19,20], CaV_2O_5, MgV_2O_5 [35,36], etc. These systems have antiferromagnetic (AFM) spin-exchange interactions along both legs and rungs, and there is also a weak interaction between two adjacent ladders. The ground state (g.s.) of these systems is a gapped SRO phase [9]. The coexisting of spin gap and long-range magnetic order in the ladder compound $LaCuO_{2.5}$ is explained considering interladder coupling [37,38].

The 1D $J_1 - J_2$ system, in the large J_2 limit, is called a zigzag ladder [4], where two chains are coupled through zigzag bonds, for example, $LiCuVO_4$ [14]. The isolated ladders like zigzag and normal ladders have been extensively studied [3,9,39–41]; however, the effect of interladder coupling on these ladders is rarely studied. Networks of the coupled zigzag ladders can form a trellis-latticelike structure as shown in Fig. 1. The trellis lattice is composed of a number of zigzag ladders coupled through normal rung bonds; alternatively, we can assume coupled normal ladders interacting through zigzaglike bond interactions. In this lattice, spin-exchange-interaction strengths J_2 and J_3 are along the leg and rung of a normal ladder, respectively, and J_1 is the zigzag bond interaction strength between two ladders as shown in Fig. 1.

In this paper, we consider only two coupled zigzag ladders and call it a *trellis ladder* because of its geometry. We also impose periodic boundary conditions along the width to mimic the trellis lattice. In various interaction limits, two coupled zigzag ladders can behave like a two-leg honeycomb ladder as considered in Ref. [42], where both J_1 and J_2 are AFM, but J_3 can be either ferromagnetic (FM) or AFM. This system shows two types of Haldane phases for the FM J_3, and columnar dimer and rung singlet phases in the presence of the AFM J_3. Normand *et al.* have considered similar coupled ladders with all three AFM J_1, J_2, and J_3 interactions [43]. For large J_2/J_1, they have noticed dimerized g.s., whereas NC long-range order (LRO) for large J_3 (J_2'). They have found Néel LRO phase in the small $J_2 < 0.4$ limit. Zinke *et al.* have shown the effect of interchain coupling on the NC g.s. of the $J_1 - J_2$ model [44], in a two-dimensional geometry. The effect

*debasmita.maiti@bose.res.in
†manoranjan.kumar@bose.res.in

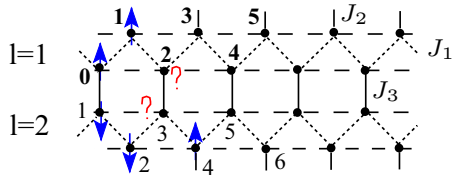

FIG. 1. Two coupled zigzag ladders form a trellis ladder. The extended lines show the extension of trellis ladder to a 2D trellis lattice structure. The arrows represent arrangement of spins and question marks represent frustrated spins. The reference site is labeled by 0 and the distances of other sites along the same ladder are shown in bold numbers, and normal numbers represent the distances on the other ladder. l represents the zigzag ladder indices.

of interladder coupling on spin gap and magnon dispersion is calculated using perturbation theory by Miyahara *et al.* [45]. They also try to model the magnetic susceptibility of $SrCu_2O_3$ and CaV_2O_5 using quantum Monte Carlo and mean-field-type scaling methods [45]. However, the system with FM J_1 and AFM J_2 and J_3 has not been studied in the ladder geometry. In this paper, we consider a spin-$\frac{1}{2}$ trellis-ladder structure, which is composed of two zigzag ladders with FM J_1 and AFM J_2, and they are coupled by AFM J_3 as shown in Fig. 1. Our main focus of this paper is to construct the quantum phase diagram (QPD) and also understand the effect of rung interaction J_3 on the various exotic phases of zigzag ladder [5]. We notice that in small $J_2/|J_1|$ limit, g.s. has collinear striped (CS) SRO on each zigzag ladder; however, spins on one zigzag ladder are aligned antiferromagnetically with respect to the spins on the other zigzag ladder [46]. The NC spin order sets in for moderate values of J_2. The presence of QLRO in the NC regime at small J_3/J_2 limit is a striking effect of the J_3. In large J_3 limit, rung dimer is the dominant g.s.

This paper is divided into four sections. In Sec. II, the model Hamiltonian and numerical method are explained. The numerical results are given in Sec. III. Linear spin-wave analysis and experimental data fitting of CaV_2O_5 are given in Secs. IV and V, respectively. All the results are discussed and summarized in Sec. VI.

II. MODEL HAMILTONIAN AND NUMERICAL METHOD

A four-legged spin-$\frac{1}{2}$ ladder made of two coupled zigzag ladders is considered as shown in Fig. 1. The exchange interactions between spins along the legs and rungs are AFM in nature. The diagonal exchange interactions J_1 in a zigzag ladder are FM. We can write an isotropic Heisenberg spin-$\frac{1}{2}$ model Hamiltonian for the trellis-ladder system as

$$\mathrm{H} = \sum_{l=1,2}\sum_{i=1}^{N/2} J_1\,\vec{S}_{l,i}\cdot\vec{S}_{l,i+1} + J_2\,\vec{S}_{l,i}\cdot\vec{S}_{l,i+2} + J_3\,\vec{S}_{1,i}\cdot\vec{S}_{2,i} + HS_i^z, \quad (1)$$

where $l = 1, 2$ are the zigzag ladder indices. $\vec{S}_{l,i}$ is the spin operator at site i on zigzag ladder l. We consider $J_1 = -1$, and J_2 and J_3 are variable AFM exchange interaction strengths. We use periodic boundary conditions along the rungs, whereas it is open along the legs of the system.

We use the density matrix renormalization group (DMRG) method to handle the large degrees of freedom in our system. This method is a state-of-the-art numerical technique for a 1D or quasi-1D system, and it is based on the systematic truncation of irrelevant degrees of freedom [47–49]. We use recently developed DMRG method where four new sites are added at every DMRG step [50]. This method, while constructing superblock, avoids the old-old operator multiplication which leads to the generation of a large number of nonzero but small matrix elements in the superblock Hamiltonian. The number of eigenvectors m, corresponding to the largest eigenvalues of the density matrix, is kept for the renormalization of operators and the Hamiltonian of the system block. We have kept m up to 400 to restrict the truncation error less than 10^{-10}. We have used system sizes up to $N = 300$ to minimize the finite size effect.

III. RESULTS

We first present an outline of the QPD which is constructed based on various quantities like correlation function $C(r)$, pitch angle θ, and bond order $C(r = 1)$. The detailed numerical and analytical calculations are discussed in the following subsections. For $J_1 = 0$, this system is composed of two isolated normal ladders and two isolated zigzag ladders for $J_3 = 0$. In $J_1 = 0$ limit, g.s. shows the formation of singlet dimers along the rungs on the normal ladder [9]. On the other hand, for $J_3 = 0$, the system shows various phases arising due to the presence of frustration in each zigzag ladder, at different exchange coupling limits. For $J_2/|J_1| < 0.25$, the g.s. of an isolated zigzag ladder has ferromagnetically ordered spins and gapless excitations. In the intermediate parameter regime, $0.25 < J_2/|J_1| < 0.67$, NC order arises in this system with a small finite spin gap [4–6,51]. The system behaves like decoupled AFM chains exhibiting QLRO in spin-spin correlation and gapless excitations in $J_2/|J_1| > 0.67$ limit [6]. We notice that if two zigzag ladders start interacting with each other through rung coupling J_3, it immediately opens a spin gap in the system. The spin gap in the CS (SRO) phase has been explicitly studied in Ref. [46]. In Sec. IV, we discuss the linear spin-wave analysis of this model. At the end, we apply this model to fit magnetic susceptibility and magnetization of CaV_2O_5 in the large J_3 limit. We also predict the specific heat curve at high temperature which can be verified experimentally.

A. Quantum phase diagram

The QPD of the Hamiltonian in Eq. (1) is shown in $J_2/|J_1|$ and $J_3/|J_1|$ parameter space, and we focus mainly on the phases in the presence of J_3. The resulting phase diagram in Fig. 2 shows two distinct phases: the CS (SRO) and NC spin order. In the small J_3 and $J_2 < 0.25$ limit, an individual zigzag ladder retains the FM arrangement of spins; however, the spins on two different zigzag ladders are aligned antiparallelly with respect to each other. Therefore, the g.s. of the whole system has effective multiplicity $S^z = 0$. The spin-spin correlation decays exponentially along each zigzag chain. This phase can be called the CS (SRO) phase. As we increase J_3, the correlation length ξ decreases. The details of this phase have

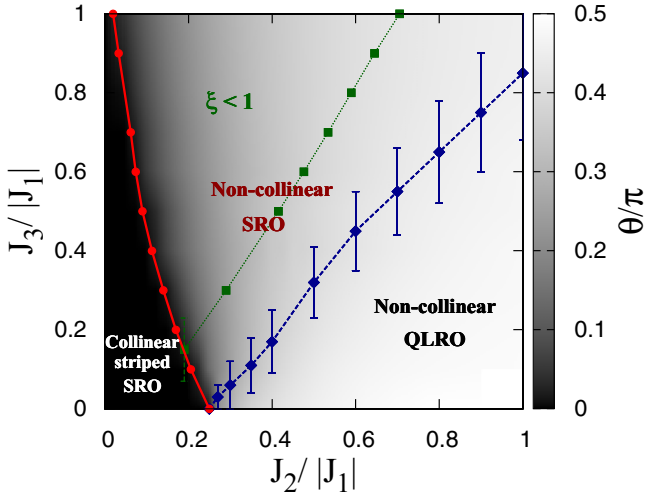

FIG. 2. The QPD of the model Hamiltonian in Eq. (1) for $H = 0$: red solid line with circles represents the boundary between CS (SRO) and NC (SRO) phases. The green dotted line with square symbols in NC (SRO) regime represents the boundary line with $\xi \approx 1$. NC (QLRO) phase lies below the blue dashed line with diamonds. The color gradient represents the pitch angle θ distribution in the $J_2 - J_3$ parameter space.

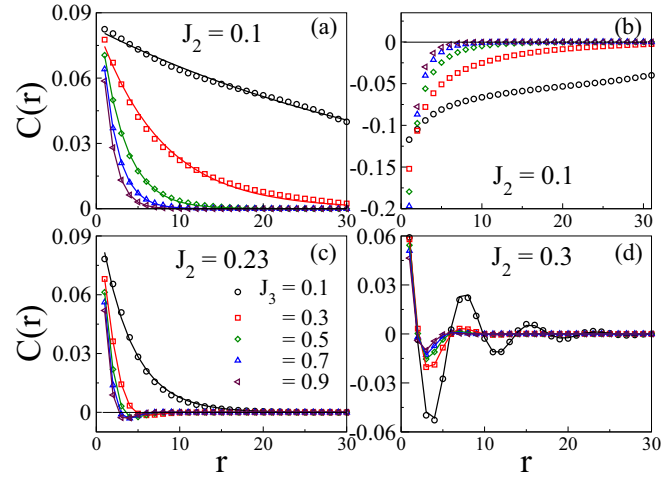

FIG. 3. The longitudinal spin-spin correlation $C(r)$ are shown along the zigzag leg with the reference spin situated on same zigzag ladder in (a), whereas $C(r)$ on the other zigzag leg is shown in (b) for $J_2 = 0.1$ and five values of $J_3 = 0.1, 0.3, 0.5, 0.7$, and 0.9 with $N = 122$. In (c) and (d), $C(r)$ in the same zigzag leg are shown for $J_2 = 0.23$ and 0.3 with same five values of J_3. The solid lines represent respective exponential fits.

been discussed already in Ref. [46]. At a higher J_3 value, even for $J_2 < 0.25$, a NC phase emerges but with small amplitude and ξ in spin-spin correlation. For $J_2 > 0.25$, spiral arrangement of spins becomes more prominent for lower J_3. In the NC regime, C(r) is either QLRO (decay following power law) called NC (QLRO), or SRO (exponentially decaying) called NC (SRO) for the small or large J_3, respectively. The θ vanishes at the boundary between CS (SRO) and NC (SRO) phases. In Fig. 2, color gradient represents θ distribution in the parameter space. The red solid line with circles represents the boundary between CS (SRO) and NC (SRO) phases in the g.s. The region above the green dotted line with square symbols represents the SRO phase where spin correlation length is confined to its neighbor, i.e., $\xi \leqslant 1$. In the large J_3 limit, the correlation strength along the rung dominates, and it tends to form singlet dimers along the rungs. The dimer phase is characterized by large energy gap, and the spin correlation is confined within the nearest neighbors ($\xi \leqslant 1$). Interestingly, for the large J_2/J_3 limit, the g.s. is in a unique NC (QLRO) phase. To best of our knowledge, QLRO phase exits with pitch angle $\theta = \pi$ or $\frac{\pi}{2}$ [5,6], whereas this system shows QLRO even with $\theta < \frac{\pi}{2}$. The NC (QLRO) phase lies below the blue dashed line with diamond symbols. The phase boundary between NC (SRO) and NC (QLRO) phases has a large error bar due to the inability to distinguish between the power law and exponential nature of $C(r)$ in this parameter regime. To verify these different phases, $C(r)$, θ, ξ, and $C(r = 1)$ are studied in detail in the following subsections.

B. Spin-spin correlation C(r)

We calculate the longitudinal spin-spin correlation $C(r) = \langle S_0^z S_r^z \rangle$, where S_0^z and S_r^z are the z component of the spin operators at the reference site 0 chosen at the middle of a zigzag chain and the site r at a distance r from zeroth spin, respectively. In Fig. 1, the distance r is shown along the same zigzag ladder with bold numerics with respect to the reference site 0, whereas normal numerics represent distances on the other zigzag leg. We note that in $J_2/|J_1| < \frac{1}{4}$ limit, all the spins are aligned parallelly on an individual zigzag ladder and have short-range longitudinal correlation for finite J_3. $C(r)$ follows an exponential behavior as shown in Fig. 3(a) for $J_2 = 0.1$ and $J_3 = 0.1, 0.3, 0.5, 0.7$, and 0.9. We notice that each zigzag ladder shows collinear arrangement of spins as $C(r) > 0$, but it decays exponentially with r, i.e.,

$$C(r) \propto \exp\left(\frac{-r}{\xi}\right). \tag{2}$$

The fitting curve represents an exponential function with correlation length ξ. Figure 3(b) shows the $C(r)$ of the same reference spin with the spins on the other zigzag leg. The negative values suggest antiparallel arrangement of spins relative to the reference spin leg. This behavior of $C(r)$ confirms the stripe nature of spin arrangement on each zigzag ladder. Therefore, we call it a striped phase. On further increase in J_2, $C(r)$ starts to oscillate at higher J_3 even at the limit $J_2 < 0.25$. For $J_2 = 0.23$, C(r) is shown in Fig. 3(c) for the same set of J_3 values. We note that NC (SRO) arises for $J_3 \geqslant 0.3$. While C(r) for $J_3 = 0.1$ is fitted by Eq. (2), C(r) for other J_3 can be fitted with the equation below:

$$C(r) \propto \exp\left(\frac{-r}{\xi}\right) \sin(\theta r + c). \tag{3}$$

The NC order can be easily noticed at lower J_3 for $J_2 > 0.25$. For $J_2 = 0.3$, C(r) is shown in Fig. 3(d) and fitted by Eq. (3). We note that ξ decreases with J_3. For moderate J_2, the NC phase follows SRO behavior, whereas it shows QLRO in the g.s. for higher $J_2 > 0.45$ but for small J_3. The transition between NC (SRO) to NC (QLRO) seems continuous, and

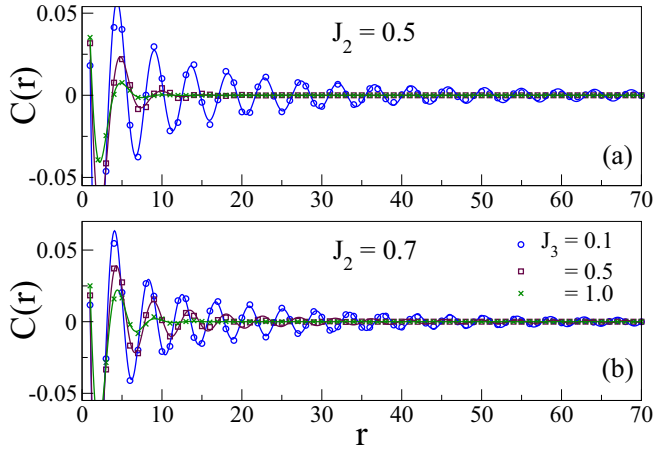

FIG. 4. For three values of $J_3 = 0.1, 0.5$ and 1.0 with $N = 298$, $C(r)$ are shown in (a) and (b) for $J_2 = 0.5$ and 0.7, respectively. The solid curves represent respective sinusoidal fits with algebraic or exponential decay.

hence it is difficult to find an accurate phase boundary. In the QLRO regime, C(r) is fitted with sinusoidal power law function written as

$$C(r) \propto r^{-\kappa} \sin(\theta r + c). \tag{4}$$

In Figs. 4(a) and 4(b), $C(r)$ are plotted for $J_2 = 0.5$ and 0.7, respectively, with $J_3 = 0.1, 0.5$, and 1.0. For $J_2 = 0.5$ and $J_3 = 0.1$, C(r) fits with the power law in Eq. (4) where $\kappa \approx 1$, whereas C(r) follows exponential decay at $J_3 = 0.5$ and 1.0 with $\xi = 2.29$ and 1.56, respectively. For $J_2 = 0.7$ and $J_3 = 0.1$ and 0.5, C(r) decays algebraically with $\kappa = 1.15$ and 1.37, respectively, but exponentially for $J_3 = 1.0$ with $\xi = 1.99$. We notice that the width of the NC (QLRO) region increases with J_2.

C. Pitch angle θ

In the NC phase, we calculate pitch angle θ from the fitting parameter in Eqs. (3) and (4). θ/π is plotted as a function of J_2 for various values of J_3, as shown in Fig. 5. θ/π versus J_2 curves are fitted with function $\theta/\pi = a[1 - e^{b(J_2 - J_2^c)}]$, where a, b, and J_2^c are the fitting parameters. J_2^c is the phase boundary point between CS (SRO) and NC (SRO) phases for a given J_2 and J_3. θ increases from 0 to $\pi/2$ with J_2. The $\theta \approx \pi/2$ region is confined to the high J_2/J_3 limit. The variation of θ is represented by the color gradient in the phase diagram in Fig. 2.

D. Correlation length ξ

The correlation length ξ extracted from fitting Eqs. (2) and (3) is a measure of correlation length in CS (SRO) and NC (SRO) phases, respectively. The nature of ξ in the CS (SRO) phase is discussed in Ref. [46]. In the NC (SRO) regime, ξ are plotted as a function of J_2 for $J_3 = 0.5, 0.6, 0.7, 0.8, 0.9$ in Fig. 6. The correlation length can be fitted by $\xi = c + dJ_2$, where c and d are the fitting parameters. We note that ξ increases with J_2/J_3. A higher value of J_2 needs more strength in J_3 to keep the same correlation length in the

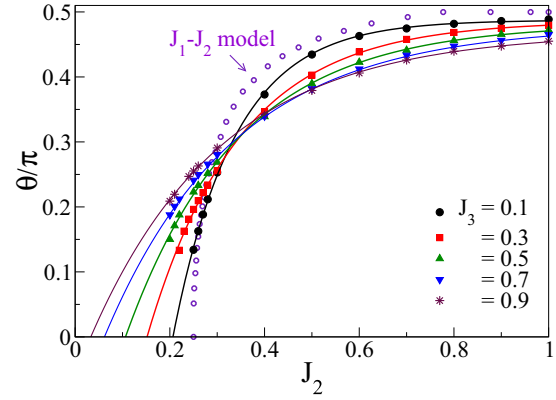

FIG. 5. The variation of pitch angle θ with J_2 are shown for five values of $J_3 = 0.1, 0.3, 0.5, 0.7$, and 0.9. The open circles represent θ for $J_1 - J_2$ spin-$\frac{1}{2}$ model on a zigzag ladder with FM J_1 and AFM J_2.

NC (SRO) phase. Surprisingly, this behavior is completely opposite in the case of the CS (SRO) phase, where higher J_2 requires lower J_3 to sustain the same correlation length [46]. When $\xi \leqslant 1$, dominant correlation strengths become confined within the three nearest neighbors among which the rung bond correlation is dominant over other two bond strengths. In fact, $\xi \leqslant 1$ represents the correlation length within nearest-neighbor distance; as per our convention of distance, both $r = 1$ and $r = 2$ are the nearest neighbors to the reference spin. In this limit, the system behaves like a collection of singlet rung dimers. The varying strength of nearest-neighbor bond correlations depending on J_2 and J_3 are discussed in the next subsection.

E. Nearest-neighbor bond correlation $C(r = 1)$

It is quite interesting to see the relative strength of nearest neighbor $C(r = 1)$ or longitudinal bond order in the parameter space. The magnitude of $C(r = 1)$ along the rung $|C^R|$, along the leg $|C^L|$, and along the zigzag leg C^D are shown for $J_2/|J_1| = 0.1, 0.4$, and 0.7 in Figs. 7(a), 7(c), and 7(d), respectively. The bonds along three directions are shown in the

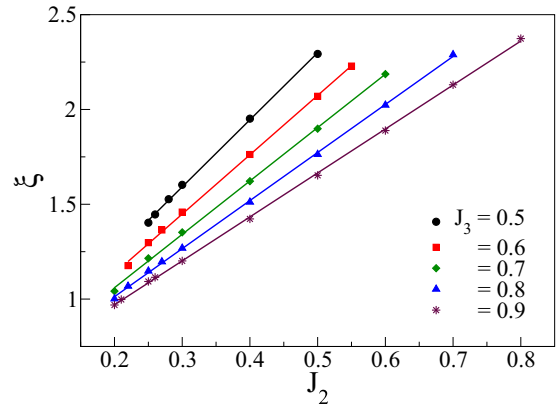

FIG. 6. In NC (SRO) phase $\xi - J_2$ curves are shown for five values of $J_3 = 0.5, 0.6, 0.7, 0.8$, and 0.9. The solid lines represent respective linear fits.

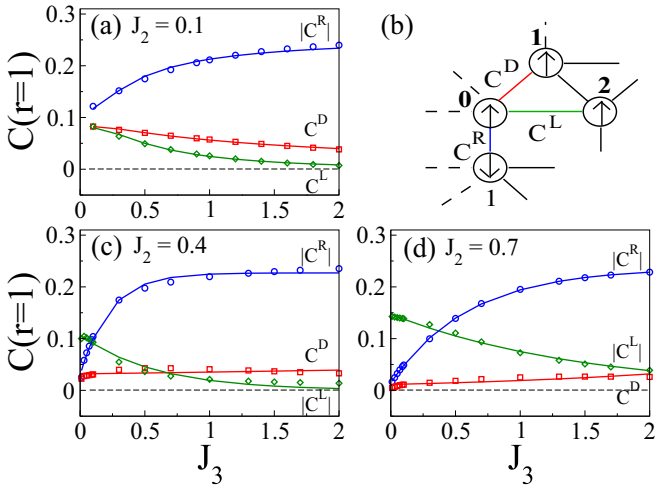

FIG. 7. Nearest-neighbor correlation function $C(r=1)$ at the middle of the zigzag ladder is shown. The $C(r=1)$ along the rung (C^R, circle), diagonal direction (C^D, square), and leg (C^L, diamond) are shown in the schematic in (b). $C(r=1)-J_3$ plots are shown for $J_2 = 0.1, 0.4$, and 0.7 in (a), (c), and (d), respectively. The lines represent respective exponential fits.

schematic Fig. 7(b). We notice that C^D and C^L have positive values for the CS (SRO) phase whereas, C^L becomes negative for the NC phase. In the NC phase, $|C^L|$ is dominant for small J_3, but $|C^R|$ dominates for $J_3 > 0.08$ and 0.38 for $J_2 = 0.4$ and 0.7, respectively. The effect of J_3 on C^D is weak, and also the magnitude of C^D is small. Therefore, we can safely conclude that major contributions of energy come from $|C^R|$ and $|C^L|$ in the NC phase. $|C^R|$ increases exponentially with J_3 and saturates to a value which is nearly equal to 0.25.

IV. LINEAR SPIN-WAVE ANALYSIS

In the CS (SRO) phase, spins on the same zigzag ladder are arranged ferromagnetically, whereas spins from different zigzag ladders are arranged antiferromagnetically to each other. We perform the linear spin-wave analysis of the Hamiltonian for this phase. We use the Holstein-Primakoff transformation to the Hamiltonian in Eq. (1). The details of the calculation are given in Appendix.

The Hamiltonian can be written in terms of bosonic operators a_j, b_j, a_j^+, and b_j^+, where a_j/a_j^+ and b_j/b_j^+ correspond to spin-up and spin-down operators or spins on legs $l = 1$ and $l = 2$, respectively. We consider only up to quadratic terms. After Fourier transformation, the resultant Hamiltonian can be written as

$$H = (2J_1 + 2J_2 - J_3)Ns^2 + \sum_k s[(2J_1(\cos k - 1) + 2J_2(\cos 2k - 1) + J_3)(a_k^+ a_k + b_k^+ b_k) + J_3(a_k^+ b_{-k}^+ + a_k b_{-k})]. \quad (5)$$

The above Hamiltonian can be transformed to a diagonal form using the Bogoliubov transformation, i.e.,

$$a_k = uc_k - vd_k^+, \qquad b_{-k}^+ = -vc_k + ud_k^+, \quad (6)$$

where $u^2 - v^2 = 1$, $u^2 + v^2 = \frac{J_k}{\sqrt{J_k^2 - J_3^2}}$ and $2uv = \frac{J_3}{\sqrt{J_k^2 - J_3^2}}$, and $J_k = 2J_1(\cos k - 1) + 2J_2(\cos 2k - 1) + J_3$. Applying Bogoliubov transformation, we get

$$H = (2J_1 + 2J_2 - J_3)Ns^2 + \sum_k \omega_k(c_k^+ c_k + d_k^+ d_k + 1), \quad (7)$$

where $\omega_k = S(\sqrt{J_k^2 - J_3^2})$.

The gs energy per bond is given by

$$\epsilon = \left(J_1 + J_2 - \frac{J_3}{2}\right)S(S+1) + \sum_k \frac{s}{2\pi}\int_0^\pi \sqrt{J_k^2 - J_3^2}\,dk. \quad (8)$$

The ϵ can be minimized using $\frac{d\omega_k}{dk} = 0$ and we find these conditions, $\cos k = \frac{-J_1}{4J_2}$ and $\cos k = \frac{-J_1}{4J_2} \pm \frac{\sqrt{(J_1+4J_2)^2 - 4J_2J_3}}{4J_2}$. The second condition $J_3 \leqslant \frac{(J_1+4J_2)^2}{4J_2}$ for any real value of $\cos k$, gives the phase boundary between CS (SRO) and NC (SRO) phases. This boundary is similar to that found by DMRG calculation.

V. FITTING EXPERIMENTAL DATA OF CaV_2O_5

There are many vanadate compounds like CaV_2O_5, MgV_2O_5, NaV_2O_5, etc., which are suspected to behave effectively like two leg ladders coupled by zigzag bonds forming a trellis-latticelike structure. Among these materials, the interladder coupling (J_1) in CaV_2O_5 is expected to be ferromagnetic. The LDA+U calculations performed by Korotin *et al.* [36] give an estimation of the J_1, J_2, and J_3 exchange interaction strengths as -28 K, 122 K, and 608 K, respectively. In this compound, V^{4+} ions have one electron the in d-orbital and behave like spin-$\frac{1}{2}$ ions. The experimental magnetic susceptibility $\chi(T)$ is taken from sample 1 and magnetization $M(H)$ is taken from sample 2 of Ref. [52] which are represented by circles in Figs. 8(a) and 8(b), respectively. The dimer model fitting of susceptibility data deviates significantly from the experimentally observed data. The experimental data is shown as a circle and the dimer fit is shown by the red dashed line in Fig. 8(a). The model Hamiltonian in Eq. (1) is used with $J_1 = -272$ K, $J_2 = 272$ K, and $J_3 = 612$ K to fit the experimental data of $M(H)$ and $\chi(T)$. The fitting curve of $\chi(T)$ shown by the black solid curve is in excellent agreement with experimental data for $T > 160$ K. As shown in Fig. 8(b), the $M-H$ curve fitted with the dimer model shown by the red dashed line is quite off at high H, whereas our model gives excellent fitting, as shown by the black solid line at $T = 200$ K. We predict the $M-H$ curve at the other three different $T = 100, 300$, and 500 K. We notice the enhancement of M as a function of T, which is quite unusual. This behavior of the $M-H$ curve can be understood in terms of large singlet-triplet gap. A moderate temperature enhances the possibility to reach higher magnetic states for a given field H.

We also predict the magnitude of specific heat C_v as a function of T for four values of magnetic field $H = 0, 10, 20, 50$ T as shown in Fig. 9. The C_v has broad peak at $T \approx 235$ K. The effect of magnetic field H is small. The C_v decreases with H, but the suppression of C_v is visible only near the peak.

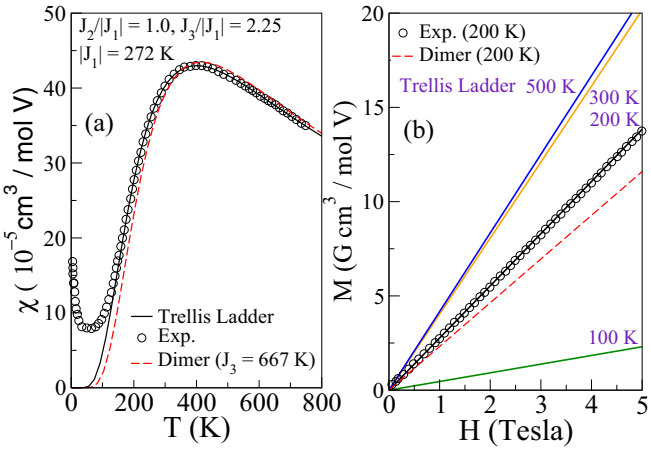

FIG. 8. (a) Magnetic susceptibility χ as a function of temperature T for CaV_2O_5 sample 1 [52] is shown by the circles. Solid curve represents the fitted curve obtained by the trellis-ladder model and dashed curve represents the fitted curve using dimer model. (b) Circles represent magnetization M versus applied magnetic field H curve at $T = 200$ K for CaV_2O_5 sample 2 [52]. The black solid line is the fit using our model and the dashed line represents the fit for a perfect dimer system at $T = 200$ K. The fitting parameters are the same as used to fit $\chi - T$ curve. The other $M - H$ plots for $T = 100$ K, 300 K, and 500 K are shown by the solid lines using the model in Eq. (1).

Initially, CaV_2O_5 was assumed to be only a dimer system with singlet-triplet energy gap $660K$ [53]. We use the model Hamiltonian in Eq. (1), and our fittings of $\chi(T)$ and $M(H)$ with same model parameters suggest that J_1 and J_2 are only $1/2$ of J_3. It is found that our predicted values of J_1 and J_2 are significantly different from the predicted values in Ref. [36], whereas the value of J_3 is similar with their calculated value using *ab initio* method in the local density approximation (LDA) + U limit.

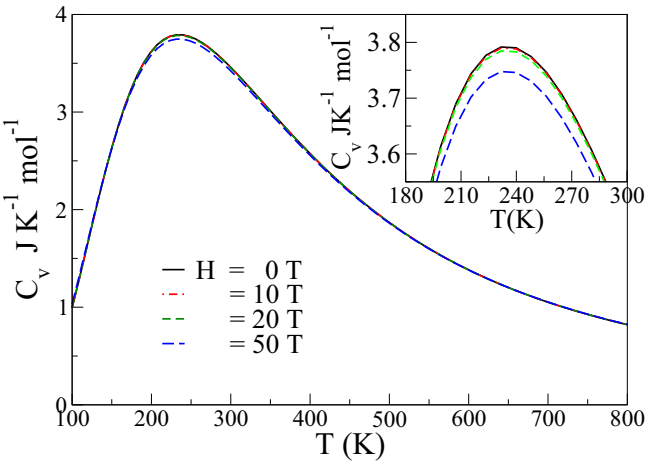

FIG. 9. Specific heat $C_v(T)$ are plotted as function of T with $J_2/|J_1| = 1.0$, $J_3/|J_1| = 2.25$, and $|J_1| = 272$ K for $H = 0$, 10, 20, and 50 T. The zoomed $C_v(T)$ near the peak are shown in the inset.

VI. DISCUSSION AND CONCLUSIONS

In this paper, we have studied the isotropic Heisenberg spin-$\frac{1}{2}$ model, given in Eq. (1), on the trellis ladder. The QPD of this model is constructed. The phase boundaries of the QPD are calculated based on the correlation function $C(r)$, pitch angle θ, and correlation length ξ using the DMRG method. Our linear spin-wave analysis of this model predicts the phase boundary of CS (SRO) and NC (SRO) phases, and it is quite consistent with our DMRG results. We also use this model to fit $\chi - T$ and $M - H$ data of CaV_2O_5, and understand the temperature T dependence of $M - H$ curves and magnetic field H dependence of $C_v - T$ curves.

In fact, our lattice system can also be mapped to two-coupled $J_1 - J_2$ Heisenberg spin-$\frac{1}{2}$ chains. Zinke *et al.* studied the effect of interchain coupling J_3 on the NC phase in a coupled 2D array of $J_1 - J_2$ spin chains using the coupled cluster theory [44]. They showed that the collinear to NC transition point J_2^c increases with J_3. However, our model shows that the critical value J_2^c decreases with J_3. This inconsistency may be because of the confined geometry or ladder structure in our case. The J_2^c value at the phase boundary of CS (SRO) and NC (SRO) phases decreases with J_3, and it can also be shown by linear spin wave analysis. As shown in Fig. 5, the variation of θ for $J_2 > 0.3$ decreases with J_3 and this trend is consistent with literature [44]—this may happen because of the deconfinement of a quasiparticle along the rung of the model. In Fig. 2 of QPD, the majority of the parameter space is a SRO phase which is basically a gapped spin-liquid phase [20,54]; however, for small values of J_3/J_2, an incommensurate (QLRO) phase appears, which is quite unique in this ladder system. The $J_1 - J_2$ spin-$\frac{1}{2}$ zigzag model in similar parameter space shows either an incommensurate (SRO) or decoupled phase [3,5]. The QLRO in the system may be induced because of the dominant effective AFM interaction along the leg.

We apply this model to understand the magnetic properties of the CaV_2O_5, and have reliable fitting of the experimental data [52]. We apply a criterion of simultaneous fitting of both experimental $\chi - T$ and $M - H$ curves. Our best fit suggests that $J_2/|J_1|$ is close to 1, and J_1 is approximately -272 K. For a given H, $M(H)$ for this system increases with T, whereas, in general, magnetization decreases with increasing temperature. We notice that in a highly gapped system, higher T allows the system to access the higher magnetic states easily; therefore, it is much easier to magnetize this system at moderate temperatures for a given H. Our calculated singlet-triplet energy gap is 459 K, whereas the dimer model predicts it as 660 K. The Knight shift and spin-lattice relaxation measurements for CaV_2O_5 show energy gaps are 464 K and 616 K, respectively [55]. Our predicted energy gap is closer to the Knight shift measurement. The modeling of $\chi(T)$ of CaV_2O_5 was done by Miyahara *et al.* using quantum Monte Carlo method, and they showed that small J_1 does not effect the magnetic $\chi(T)$, as shown in Fig. 6 of Ref. [45]. They estimated the value of $J_1 = 45$ K, $J_2 = 67$ K, and $J_3 = 672$ K. Johnston *et al.* treated this system as collection of dimers, and extracted the value of $J_3 = 667$ K with small J_1 and J_2 [52]. Korotin *et al.* also calculated the value of $J_1 = -28$ K,

$J_2 = 122$ K, and $J_3 = 608$ K; however, their calculation also assumes other types of interactions [36]. Our simultaneous fitting of experimental $\chi - T$ and $M - H$ data also suggests it as a dominant dimer with $J_3 = 612$ K, but $-J_1$ and J_2 are only about half in magnitude of J_3.

In summary, we study the QPD of the model Hamiltonian in Eq. (1) on the trellis ladder. We show that J_3 plays an important role to localize the system. This system shows interesting CS (SRO) and NC (QLRO), which is rare in ladderlike structures. This model Hamiltonian is used to fit the experimental magnetic properties of CaV_2O_5 and we also show that the interactions J_1 and J_2 are much larger than earlier predicted values, and J_1 is ferromagnetic in nature. In many zigzag ladder systems like $LiCuVO_4$ [14], Li_2CuZrO_4 [15], Li_2CuSbO_4 [16], etc., where three-dimensional ordering occurs at low T, this model can be applied to understand the effect of interladder coupling in the system. We have also predicted the $M - H$ and $C_v - T$ curves which can be verified experimentally.

ACKNOWLEDGMENTS

M.K. thanks Prof. Z. G. Soos for useful discussions and also thanks DST India for a Ramanujan Fellowship No. SR/S2/RJN-69/2012 and DST India for funding computation facility through SNB/MK/14-15/137. Debasmita thanks Dayasindhu Dey for help in linearized spin-wave-theory calculations.

APPENDIX

For up spins, the Holstein-Primakoff transformations take the form

$$\begin{aligned} S^z_{Aj} &= s - a^+_j a_j, \\ S^+_{Aj} &= \sqrt{(2s - a^+_j a_j)}\, a_j, \\ S^-_{Aj} &= a^+_j \sqrt{(2s - a^+_j a_j)}, \end{aligned} \tag{A1}$$

For the down spin:

$$\begin{aligned} S^z_{Bj} &= -s + b^+_j b_j, \\ S^+_{Bj} &= a^+_j \sqrt{(2s - a^+_j a_j)}, \\ S^-_{Bj} &= \sqrt{(2s - a^+_j a_j)}\, a_j. \end{aligned} \tag{A2}$$

We use the linear approximation at classical limit,

$$\begin{aligned} S^z_{Aj} &= s - a^+_j a_j, \\ S^+_{Aj} &= \sqrt{2s} a_j, \\ S^-_{Aj} &= \sqrt{2s} a^+_j, \end{aligned} \tag{A3}$$

for spin up, and for spin down:

$$\begin{aligned} S^z_{Bj} &= s - b^+_j b_j, \\ S^+_{Bj} &= \sqrt{2s} b^+_j, \\ S^-_{Bj} &= \sqrt{2s} b_j. \end{aligned} \tag{A4}$$

In terms of bosonic operators, the Hamiltonian takes the form up to quadratic order as

$$\begin{aligned} H = {} & (2J_1 + 2J_2 - J_3)Ns^2 + \sum_j s[[J_1(a^+_j a_{j+1} + b^+_j b_{j+1}) \\ & + J_2(a^+_j a_{j+2} + b^+_j b_{j+2}) + J_3 a_j b_j + \text{H.c.}] \\ & - (J_1 + J_2)(a^+_j a_j + b^+_j b_j) - J_1(a^+_{j+1} a_{j+1} + b^+_{j+1} b_{j+1}) \\ & + J_2(a^+_{j+2} a_{j+2} + b^+_{j+2} b_{j+2}) + J_3(a^+_j a_j + b^+_j b_j)]. \end{aligned} \tag{A5}$$

Fourier transforms of the bosonic operators are

$$\begin{aligned} a_j &= \sum_k \exp(-ikj) a_k, \\ a^+_j &= \sum_k \exp(ikj) a^+_k. \end{aligned} \tag{A6}$$

[1] K. Okamoto and K. Nomura, Phys. Lett. A **169**, 433 (1992).
[2] F. D. M. Haldane, Phys. Rev. B **25**, 4925 (1982).
[3] S. R. White and I. Affleck, Phys. Rev. B **54**, 9862 (1996).
[4] R. Chitra, S. Pati, H. R. Krishnamurthy, D. Sen, and S. Ramasesha, Phys. Rev. B **52**, 6581 (1995).
[5] M. Kumar, A. Parvej, and Z. G. Soos, J. Phys.: Condens. Matter **27**, 316001 (2015).
[6] Z. G. Soos, A. Parvej, and M. Kumar, J. Phys.: Condens. Matter **28**, 175603 (2016).
[7] C. K. Majumdar and D. K. Ghosh, J. Math. Phys. **10**, 1388 (1969).
[8] B. S. Shastry and B. Sutherland, Phys. Rev. Lett. **47**, 964 (1981).
[9] S. R. White, R. M. Noack, and D. J. Scalapino, Phys. Rev. Lett. **73**, 886 (1994).
[10] A. V. Chubukov, Phys. Rev. B **44**, 4693 (1991).
[11] S. Furukawa, M. Sato, S. Onoda, and A. Furusaki, Phys. Rev. B **86**, 094417 (2012).
[12] M. E. Zhitomirsky and H. Tsunetsugu, Europhys. Lett. **92**, 37001 (2010).
[13] A. Parvej and M. Kumar, Phys. Rev. B **96**, 054413 (2017).
[14] M. Mourigal, M. Enderle, B. Fåk, R. K. Kremer, J. M. Law, A. Schneidewind, A. Hiess, and A. Prokofiev, Phys. Rev. Lett. **109**, 027203 (2012).
[15] S.-L. Drechsler, O. Volkova, A. N. Vasiliev, N. Tristan, J. Richter, M. Schmitt, H. Rosner, J. Málek, R. Klingeler, A. A. Zvyagin, and B. Büchner, Phys. Rev. Lett. **98**, 077202 (2007).
[16] S. E. Dutton, M. Kumar, M. Mourigal, Z. G. Soos, J.-J. Wen, C. L. Broholm, N. H. Andersen, Q. Huang, M. Zbiri, R. Toft-Petersen, and R. J. Cava, Phys. Rev. Lett. **108**, 187206 (2012).
[17] N. Maeshima, M. Hagiwara, Y. Narumi, K. Kindo, T. C. Kobayashi, and K. Okunishi, J. Phys.: Condens. Matter **15**, 3607 (2003).
[18] A. W. Sandvik, E. Dagotto, and D. J. Scalapino, Phys. Rev. B **53**, R2934 (1996).
[19] D. C. Johnston, J. W. Johnson, D. P. Goshorn, and A. J. Jacobson, Phys. Rev. B **35**, 219 (1987).
[20] E. Dagotto and T. M. Rice, Science **271**, 618 (1996).

[21] S. E. Dutton, M. Kumar, Z. G. Soos, C. L. Broholm, and R. J. Cava, J. Phys.: Condens. Matter **24**, 166001 (2012).
[22] M. Kumar, S. E. Dutton, R. J. Cava, and Z. G. Soos, J. Phys.: Condens. Matter **25**, 136004 (2013).
[23] O. S. Volkova, I. S. Maslova, R. Klingeler, M. Abdel-Hafiez, Y. C. Arango, A. U. B. Wolter, V. Kataev, B. Büchner, and A. N. Vasiliev, Phys. Rev. B **85**, 104420 (2012).
[24] B. Koteswararao, A. V. Mahajan, F. Bert, P. Mendels, J. Chakraborty, V. Singh, I. Dasgupta, S. Rayaprol, V. Siruguri, A. Hoser, and S. D. Kaushik, J. Phys.: Condens. Matter **24**, 236001 (2012).
[25] C. K. Majumdar and D. K. Ghosh, J. Math. Phys. **10**, 1399 (1969).
[26] T. Tonegawa and I. Harada, J. Phys. Soc. Jpn. **56**, 2153 (1987).
[27] K. Kuboki and H. Fukuyama, J. Phys. Soc. Jpn. **56**, 3126 (1987).
[28] T. Hamada, J.-i. Kane, S.-i. Nakagawa, and Y. Natsume, J. Phys. Soc. Jpn. **57**, 1891 (1988).
[29] R. Bursill, G. A. Gehring, D. J. J. Farnell, J. B. Parkinson, T. Xiang, and C. Zeng, J. Phys.: Condens. Matter **7**, 8605 (1995).
[30] D. Allen and D. Sénéchal, Phys. Rev. B **55**, 299 (1997).
[31] C. Itoi and S. Qin, Phys. Rev. B **63**, 224423 (2001).
[32] M. Hase, H. Kuroe, K. Ozawa, O. Suzuki, H. Kitazawa, G. Kido, and T. Sekine, Phys. Rev. B **70**, 104426 (2004).
[33] H. T. Lu, Y. J. Wang, S. Qin, and T. Xiang, Phys. Rev. B **74**, 134425 (2006).
[34] M. Kumar, S. Ramasesha, and Z. G. Soos, Phys. Rev. B **81**, 054413 (2010).
[35] M. A. Korotin, I. S. Elfimov, V. I. Anisimov, M. Troyer, and D. I. Khomskii, Phys. Rev. Lett. **83**, 1387 (1999).
[36] M. A. Korotin, V. I. Anisimov, T. Saha-Dasgupta, and I. Dasgupta, J. Phys.: Condens. Matter **12**, 113 (2000).
[37] B. Normand and T. M. Rice, Phys. Rev. B **54**, 7180 (1996).
[38] M. Troyer, M. E. Zhitomirsky, and K. Ueda, Phys. Rev. B **55**, R6117 (1997).
[39] J. Almeida, M. A. Martin-Delgado, and G. Sierra, Phys. Rev. B **76**, 184428 (2007).
[40] T. Vekua, G. I. Japaridze, and H.-J. Mikeska, Phys. Rev. B **67**, 064419 (2003).
[41] C. E. Agrapidis, S.-L. Drechsler, J. van den Brink, and S. Nishimoto, Phys. Rev. B **95**, 220404(R) (2017).
[42] Q. Luo, S. Hu, J. Zhao, A. Metavitsiadis, S. Eggert, and X. Wang, Phys. Rev. B **97**, 214433 (2018).
[43] B. Normand, K. Penc, M. Albrecht, and F. Mila, Phys. Rev. B **56**, R5736 (1997).
[44] R. Zinke, S.-L. Drechsler, and J. Richter, Phys. Rev. B **79**, 094425 (2009).
[45] S. Miyahara, M. Troyer, D. Johnston, and K. Ueda, J. Phys. Soc. Jpn. **67**, 3918 (1998).
[46] D. Maiti and M. Kumar, J. Magn. Magn. Mater. **486**, 165266 (2019).
[47] S. R. White, Phys. Rev. Lett. **69**, 2863 (1992).
[48] K. A. Hallberg, Adv. Phys. **55**, 477 (2006).
[49] U. Schollwöck, Rev. Mod. Phys. **77**, 259 (2005).
[50] M. Kumar, Z. G. Soos, D. Sen, and S. Ramasesha, Phys. Rev. B **81**, 104406 (2010).
[51] M. Kumar and Z. G. Soos, Phys. Rev. B **88**, 134412 (2013).
[52] D. C. Johnston, M. Troyer, S. Miyahara, D. Lidsky, K. Ueda, M. Azuma, Z. Hiroi, M. Takano, M. Isobe, Y. Ueda, M. A. Korotin, V. I. Anisimov, A. V. Mahajan, and L. L. Miller, arXiv:cond-mat/0001147.
[53] M. Onoda and N. Nishiguchi, J. Solid State Chem. **127**, 359 (1996).
[54] F. Mila, Eur. J. Phys. **21**, 499 (2000).
[55] H. Iwase, M. Isobe, Y. Ueda, and H. Yasuoka, J. Phys. Soc. Jpn. **65**, 2397 (1996).